JOURNAL OF AIRCRAFT
Vol. 47, No. 1, January–February 2010

Vortex Dynamics of Free-to-Roll Slender and Nonslender Delta Wings

N. T. Gresham,* Z. Wang,† and I. Gursul‡
University of Bath, Bath, England BA2 7AY, United Kingdom

DOI: 10.2514/1.45425

Experiments were conducted on various free-to-roll delta wings with sweep angles in the range of 40–70 deg in a wind tunnel. For low sweep angles, nonzero trim angles are observed until the wing stalls after which the trim angle becomes zero. The magnitude of the roll trim angle decreases with increasing sweep angle and almost disappears for the most slender wing. In a certain range of sweep angles, and just before the stall, large amplitude self-induced roll oscillations with nonzero mean were observed for thin wings with sharp leading edges for which separation point is fixed. Two different regions of angle of attack with free-to-roll oscillations were found for certain sweep angles. Velocity measurements suggest that the oscillations are initiated by the increasing proximity of the shear layers as the angle of attack is increased. Possible mechanisms of the self-induced roll oscillations based upon the phase-averaged velocity measurements have been proposed, incorporating varying vortex size and strength as well as the movement of the shear-layer reattachment locations. Hysteresis and time lag effects are significant even though typical dimensionless frequencies are very low.

Nomenclature

A	=	wing area
b	=	wingspan
c	=	wing chord
I_{xx}	=	moment of inertia about x axis
Re	=	Reynolds number, $\rho U_\infty c/\mu$
St	=	Strouhal number, fc/U_∞
t	=	thickness
U_∞	=	freestream velocity
x	=	streamwise coordinate
α	=	angle of attack
Λ	=	leading-edge sweep angle
μ	=	viscosity of air
ρ	=	density of air
Φ	=	roll angle
Φ_{max}	=	maximum roll angle
Φ_{mean}	=	mean roll angle
Φ_{min}	=	minimum roll angle

I. Introduction

UNSTEADY aerodynamics of delta wings in roll motion are important for various applications including high-speed civil transport, spacecraft, fighter aircraft, unmanned combat air vehicles, and micro air vehicles. Most of the knowledge on aerodynamics of rolling motion is on slender wings [1–7]. Self-induced roll oscillation of slender delta wings, known as wing rock [1–3], is the best known aspect of the roll motion aerodynamics. Wing rock has been observed for slender wings with sweep angle $\Lambda \geq 75$ deg and with corresponding mean roll angle of zero. Previous observations have suggested that the proximity of the leading-edge vortices to each other may be important. Arena and Nelson [2] suggested that a possible mechanism to sustain the wing rock motion is the time lag in the position of the vortices normal to the wing surface.

Previous studies on slender delta wings also revealed the existence of critical states [4] and the importance of vortex breakdown [5,6]. The existence of equilibrium positions at nonzero roll angles is another curious aspect. Jenkins et al. [4] showed that a delta wing configuration with 65 deg sweep angle had multiple stable trim points in roll. In the free-to-roll experiments, the model is released from an initial roll angle and then is set free to roll. The phase plane (roll rate versus roll angle) trajectories, corresponding to two free-to-roll time histories for the 65 deg wing at $\alpha = 30$ deg, showed very different behavior. For the initial roll angle $\Phi_0 = -58.3$ deg, the trajectory finds the stable equilibrium point at zero roll angle, whereas for $\Phi_0 = 53.1$ deg, the final equilibrium position is around $\Phi = 21$ deg. The existence of equilibrium positions at nonzero roll angles was also confirmed at other angles of attack for this slender delta wing configuration. The measured static rolling moment becomes zero at these nonzero trim angles, and it is believed that asymmetric vortex breakdown is behind this behavior.

Somewhat different type of roll oscillations is observed for nonslender delta wings. Around the stall angle, self-excited roll oscillations [8–10] were observed for a sweep angle of $\Lambda = 45$ deg. These oscillations are unusual because not only are they observed for a nonslender wing, but also because the mean roll angle is nonzero. Only the wings with round leading edges exhibited roll oscillations, but no oscillations were observed for a wing with sharp leading edges for the same sweep angle. Ericsson [11] speculated that wing rock of nonslender delta wings can occur only if the wing has a rounded leading edge. However, recent experiments for wings with sweep angle of $\Lambda = 50$ deg in a different facility [12,13] showed that round leading edge is not necessary and roll oscillations can develop for sharp leading edges as well. Free-to-roll oscillations were found for both a thick wing with thickness-to-chord ratio $t/c = 10\%$ and round leading edges and a thin wing with $t/c = 1.5\%$ and sharp leading edges, both with $\Lambda = 50$ deg. The time history of the roll angle during these oscillations is shown in Figs. 1a and 1b, respectively, and it can be seen that the sharp leading-edged wing oscillated at lower amplitude and higher frequency; whereas both wings exhibited nonzero roll angles.

The oscillations are observed around the stall angle in which the reattachment of asymmetric flows is the most important factor [13]. If the leading edge is rounded (hence, the separation line is not fixed), unsteady separation at the leading edge might also contribute to the roll oscillations. Self-excited roll oscillations of nonslender wings appear to be more complex in their aerodynamic origins than slender

Received 13 May 2009; revision received 10 July 2009; accepted for publication 10 July 2009. Copyright © 2009 by Ismet Gursul. Published by the American Institute of Aeronautics and Astronautics, Inc., with permission. Copies of this paper may be made for personal or internal use, on condition that the copier pay the $10.00 per-copy fee to the Copyright Clearance Center, Inc., 222 Rosewood Drive, Danvers, MA 01923; include the code 0021-8669/10 and $10.00 in correspondence with the CCC.

*Postgraduate Student, Department of Mechanical Engineering.
†Academic Fellow, Research Councils United Kingdom, Department of Mechanical Engineering.
‡Professor, Department of Mechanical Engineering. Associate Fellow AIAA.

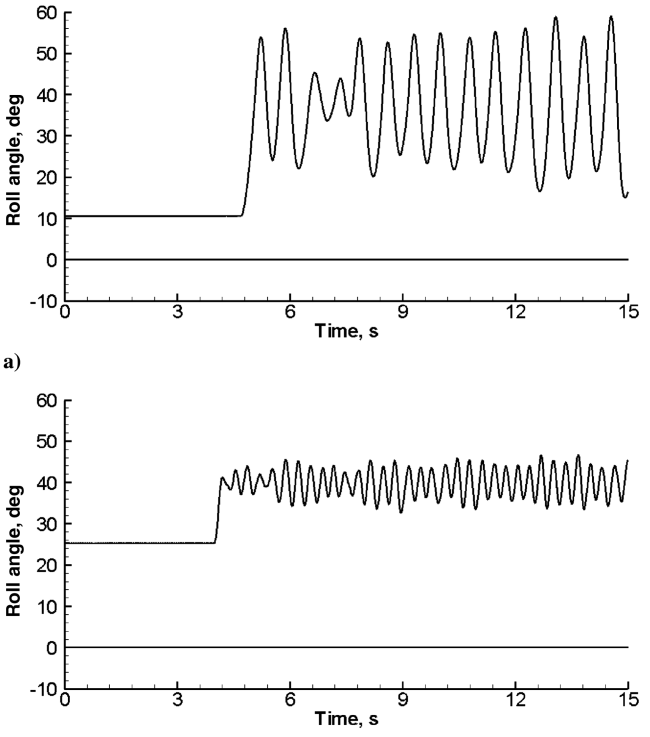

Fig. 1 Time history of roll angle with $\Lambda = 50$ deg: a) thick wing with round leading edges at $\alpha = 27.5$ deg, and b) thin wing with sharp leading edges at $\alpha = 22.5$ deg.

wing rock. Flow physics of free-to-roll dynamics of nonslender wings is not completely understood yet. The main objective of this paper is to present results of an experimental investigation on free-to-roll delta wings with various sweep angles. The nature of self-excited roll oscillations and corresponding vortex topology is discussed.

Previous work [8–13] also confirmed that, even when there are no roll oscillations, free-to-roll nonslender delta wings may have trim positions at nonzero roll angles. In other words, zero roll angle is not stable to roll disturbances. Although this is similar to the observations for a slender wing [4] with sweep angle $\Lambda = 65$ deg, the flow physics might be different. Although it is believed that asymmetric vortex breakdown is behind the nonzero trim angles for slender wings, it is not clear whether this is also the case for nonslender wings. It is suspected that the nonzero trim angles are related to asymmetric reattachment of the separated flows. It is recalled that reattachment on the wing surface is typical for nonslender wings [14]. It would be interesting to study this behavior as a function of sweep angle and investigate the transition from slender to nonslender wings. This is the second objective of this paper.

In summary, we have two major goals in this study: 1) to investigate further the effect of sweep angle on self-excited roll oscillations, to examine the corresponding vortex topology, and to endeavour to provide a suitable explanation for why the oscillations occur; and 2) to investigate the nonzero trim angles as a function of sweep angle. We have performed wind-tunnel experiments on various wing models, which include a thick wing with round leading edges and 50 deg sweep angle, and various thin wings with sharp leading edges and sweep angles from 40 to 70 deg. Roll response of the free-to-roll wings as well as corresponding vortex topologies are reported by means of the particle image velocimetry (PIV) measurements.

II. Experimental Apparatus and Procedures

A. Closed-Loop Wind Tunnel

The high-speed section of the closed-return wind tunnel at the University of Bath was used for all the testing. The working section of the wind tunnel has dimensions of $2.13 \times 1.52 \times 2.7$ m and can operate at speeds of up to 50 ms^{-1}. All the experiments in this study were conducted at a tunnel speed of 30 ms^{-1}, and the maximum blockage for the wind-tunnel models was approximately 2% at the maximum angle of attack $\alpha = 50$ deg. Figure 2 shows the working section layout, including the high-alpha rig, which allows the angle of attack to be varied as the wind tunnel is running.

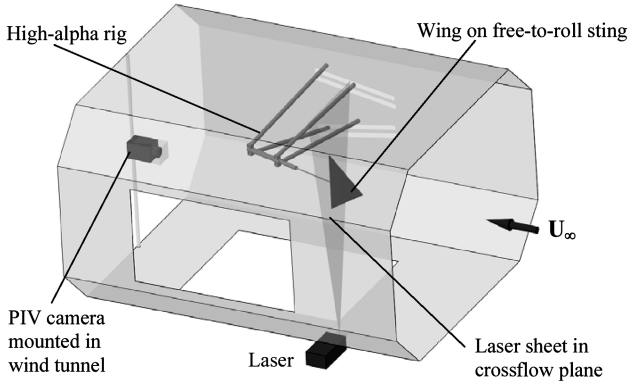

Fig. 2 Layout of high-speed working section of the University of Bath wind tunnel.

B. Free-to-Roll Device

Figure 3a shows a schematic of the free-to-roll device that was used for the experiments performed. It consisted of a shaft supported in greased bearings and so was free to rotate with minimal friction. One end of the shaft was attached to a potentiometer, which output a varying voltage, linearly dependent on the roll angle, whereas the other end of the shaft attached to the sting upon which the wing was supported. The sting for the thick wing simply entered into the wing itself, so that both surfaces were clean, whereas the support for the thin wings is depicted in Fig. 3b, which shows the free-to-roll device,

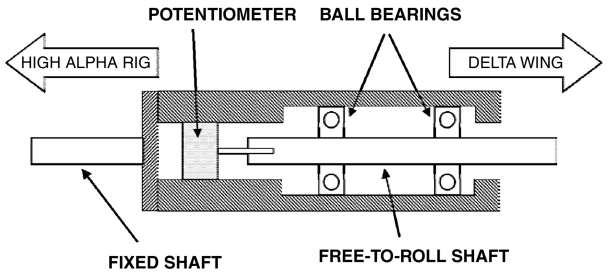

a)

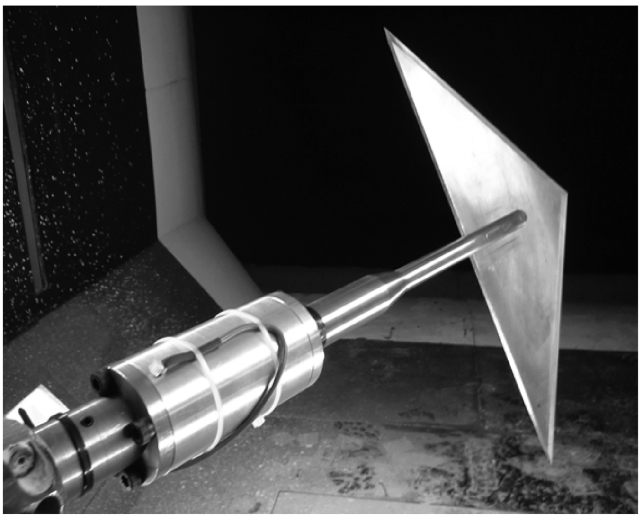

b)

Fig. 3 Free-to-roll device in wind tunnel: a) schematic, and b) picture.

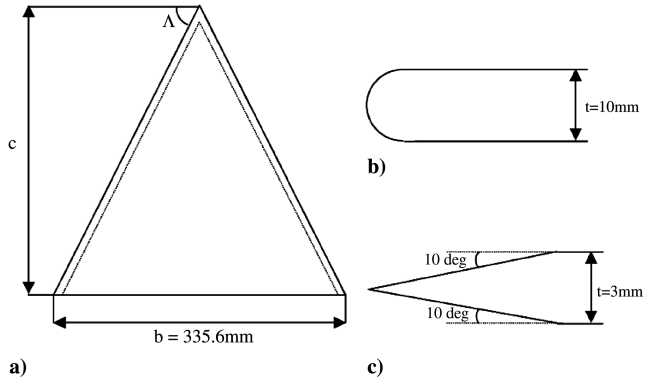

Fig. 4 a) Generic delta wing planform: b) semi-circular (round), and c) sharp leading edge profiles (not to scale).

wing support and the pressure surface of the wing. The suction surface of the wing was flat with no protrusions. The output from the potentiometer was fed to the computer via an A/D converter at a rate of 250 Hz with an estimated uncertainty of ± 1 deg. The stings used for all the models on the free-to-roll device were in line with the roll axis of the wings themselves and so there was no coning motion, just pure roll. For roll angle time histories and subsequent calculations, the roll angle was acquired for 90 s at the desired angles of attack. No initial roll angle was imposed upon any of the wings.

C. Models

Figure 4a shows a generic delta wing planform for all the models tested. Firstly a thick wing of $\Lambda = 50$ deg was fabricated from high-density polyethylene (HDPE) with round leading edges, as shown in Fig. 4b. Thin, aluminum wings of $\Lambda = 40, 45, 50, 52.5, 55, 57.5, 60, 65$, and 70 deg were also made to investigate the effect of sweep angle, all with the same span, thickness, and sharp leading edges. The profile of the leading edges is shown in Fig. 4c, which shows the double 10 deg bevel used to fix the separation point. A summary of the physical properties of the wings tested is shown in Table 1. The moment of inertia about the roll axis for each wing was calculated using a CAD software, which had been calibrated using the measured masses of the wings, and includes the moment of inertia of the sting used. The Reynolds numbers (based on wing root chord length) are similar to flight conditions for unmanned air vehicles operating at low-transitional Reynolds numbers. The models were painted matte black to reduce reflections created from the laser during the PIV tests.

D. Particle Image Velocimetry System

A dual 120 mJ Nd:YAG digital particle image velocimetry (PIV) system was used to capture the crossflow velocity field, with seeding provided by a smoke machine placed in the low-speed section of the wind tunnel. The maximum repetition rate of the PIV system was 3.75 Hz in the cross-correlation mode. An interrogation window size of 32×32 pixels was used to produce velocity vectors for further processing. The effective grid size varied from 1.2 to 1.45 mm in these measurements. Both the time and phase-averaged velocity measurements were performed for the static and dynamic wings, respectively. Sequences of 1000 images were taken at a time to obtain a time-averaged field and a fast Fourier transform correlation algorithm was used to obtain the velocity vectors. The measurement uncertainty for the velocity is estimated as 2% of the freestream velocity. The setup of the laser and mirror in the wind tunnel is shown in Fig. 2, and measurements were taken in crossflow planes at $x/c = 0.25$ and $x/c = 0.5$, with two separate tests needed to cover the measurement domain in the latter case. For experiments with static wings, tests were performed while the wing was clamped at the desired roll angle, and dynamic tests were performed with the clamp removed. In the dynamic cases, an external trigger card was used to trigger the PIV system as the wing rolled through a user-defined roll angle, with the roll angle either increasing or decreasing. The timing of the triggers was logged together with the time history of the roll angle. An error of ± 1 deg in the trigger angle existed in these measurements.

III. Results and Discussion

As previous work suggested that round leading edges might amplify the self-excited roll oscillations, we investigated the thick wing in detail first. Vortex topology from the PIV measurements was studied to understand the flow physics. Then, we investigated the roll behavior of slender and nonslender delta wings with sharp leading edges. Velocity measurements were performed for selected cases.

A. Velocity Field for Round Leading Edges

Figures 5 and 6 show the crossflow velocity field and streamlines, respectively, for the thick wing in motion at $\alpha = 28$ deg (for which large roll oscillations are observed) and $x/c = 0.25$. In Fig. 5, every other vector is omitted for clarity. The roll angles at which the phase-averaged measurements were taken are shown in the inset. It is seen that there is some amplitude modulation of the roll oscillations. One roll angle near the minimum and one roll angle near the maximum were investigated. In addition, the mean-roll angle for increasing and decreasing roll angle make up the four instants shown in Fig. 5. The velocity field in Fig. 5 shows the separated shear layer originating from the right-hand leading edge, whereas the separated flow near the left-hand leading edge is very small. Near the maximum roll angle and the mean roll angle for decreasing roll, the right-hand shear layer is very close to the wing surface. It moves farther away from the wing surface at the minimum roll angle (part iii) and the mean roll angle for increasing roll (part iv). Figure 5 also shows the movement of the right-hand shear layer reattachment point, and how an area of reattached flow exists near Φ_{max}, but is not evident near Φ_{min} or at Φ_{mean} as the roll angle increases. As near Φ_{max} the shear layer is much closer to the wing surface, this presumably generates the lift on that wing half to drive the wing back in the other direction. There appears to be a time lag in the development of the flow.

Corresponding streamline patterns in Fig. 6 also show that the separated region on the right-hand side is much larger than that on the left-hand side. Dividing streamlines between the freestream and separated region as well as the saddle point in the crossflow plane are clearly seen. This figure also illustrates the hysteresis when the streamline patterns are compared for the mean angles for increasing and decreasing roll angle. This hysteresis effect is more pronounced at a streamwise station further downstream ($x/c = 0.5$) as shown in Fig. 7 (every other vector is omitted for clarity). This figure shows the

Table 1 Properties of wings tested

Λ, deg	50	40	45	50	52.5	55	57.5	60	65	70
Leading edge	Round	Sharp	Sharp	Sharp	Sharp	Sharp	Sharp	Sharp	Sharp	Sharp
c, mm	200	140.8	167.8	200	218.7	239.7	263.4	290.7	359.9	461.1
b, mm	335.6	335.6	335.6	335.6	335.6	335.6	335.6	335.6	335.6	335.6
A, m^2	3.36×10^{-2}	2.37×10^{-2}	2.82×10^{-2}	3.36×10^{-2}	3.67×10^{-2}	4.02×10^{-2}	4.42×10^{-2}	4.88×10^{-2}	6.04×10^{-2}	7.74×10^{-2}
t/c, %	10	2.13	1.79	1.50	1.37	1.25	1.14	1.03	0.83	0.65
I_{xx}, kgm^2	3.08×10^{-3}	0.79×10^{-3}	0.94×10^{-3}	1.21×10^{-3}	1.24×10^{-3}	1.37×10^{-3}	1.42×10^{-3}	1.76×10^{-3}	2.08×10^{-3}	2.66×10^{-3}
Material	HDPE	Al	Al	Al	Al	Al	Al	Al	Al	Al
Re	4.11×10^5	2.89×10^5	3.45×10^5	4.11×10^5	4.49×10^5	4.92×10^5	5.30×10^5	5.97×10^5	7.39×10^5	9.27×10^5

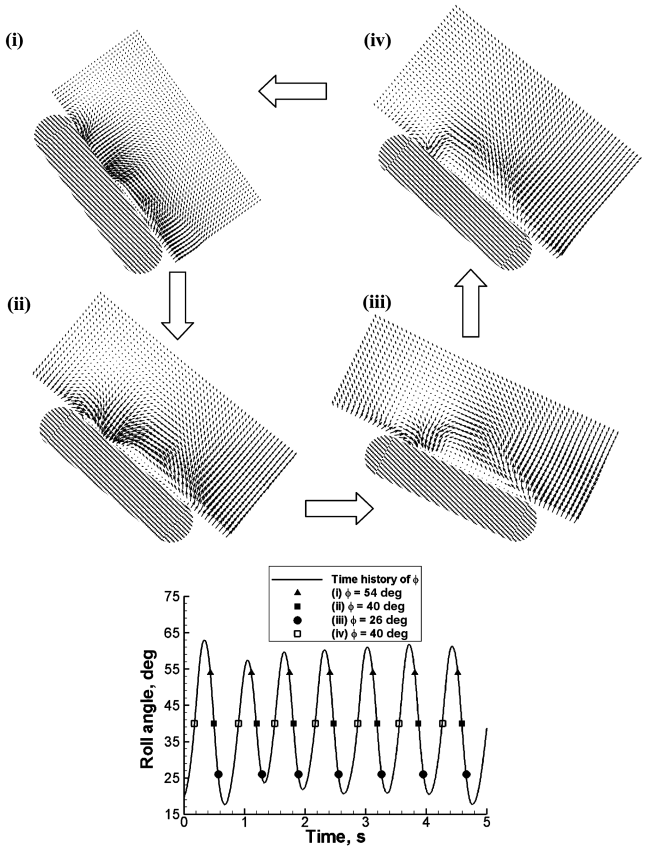

Fig. 5 Phase-averaged crossflow velocity and timing diagram corresponding to images for thick wing at $x/c = 0.25$ and $\alpha = 28$ deg.

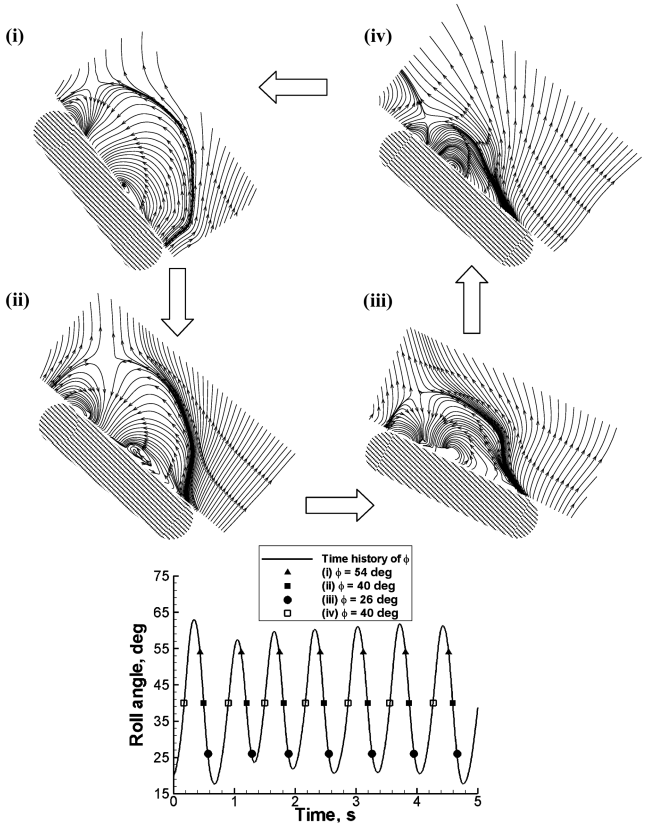

Fig. 6 Crossflow streamlines and timing diagram corresponding to images for thick wing at $x/c = 0.25$ and $\alpha = 28$ deg.

three different flow structures possible at the mean roll angle depending on whether the wing is static, Φ is decreasing, or Φ is increasing. These different flow structures indicate the presence of a time lag, without which the motion would not occur. Figures 7a and 7b show that the structures in these two cases are very similar, though with a slightly larger area of reattached flow in Fig. 7b. In this case, the right-hand vortical structure must be generating more lift than the left-hand wing half. A significant difference exists for Φ increasing, with the right-hand shear layer being much further from the wing surface. In this instance, the left-hand vortex must be generating more lift to drive the motion. At this streamwise station, the vortical flow developing on the left-hand side is more visible. In all cases in Fig. 7, the left-hand vortex is compact and approximately the same size. Vortex breakdown is unlikely to develop on the left-hand side, however, we do not have streamwise velocity data to substantiate this. The right-hand vortical flow is expected to have breakdown at the apex at all roll angles. Although a general understanding of the vortical flow during the roll oscillations is achieved, the role of the

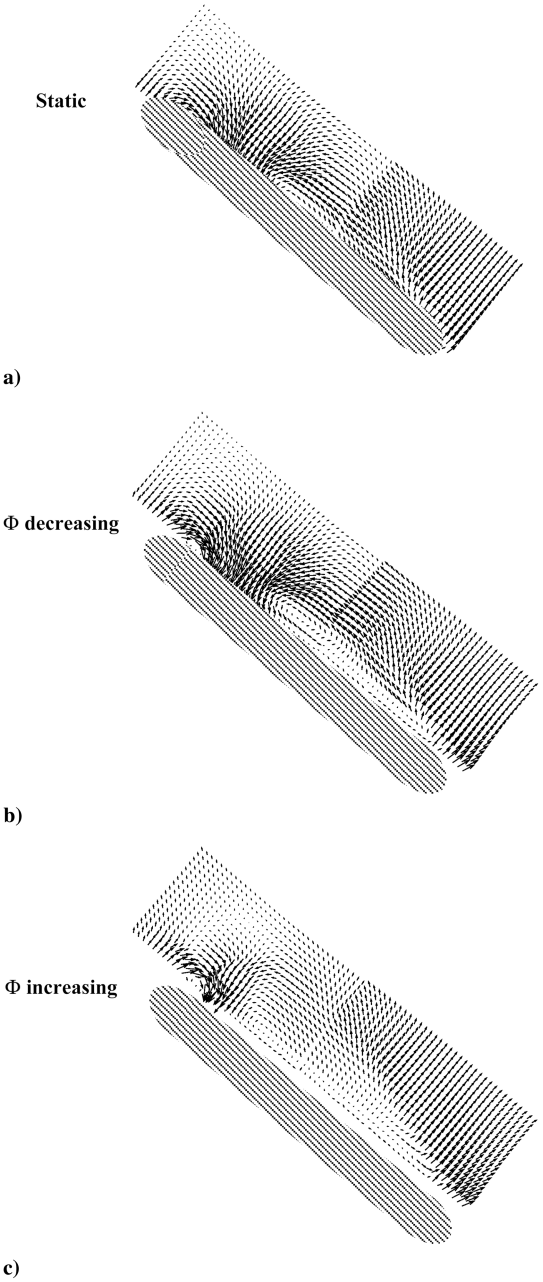

Fig. 7 Crossflow velocity fields at $x/c = 0.5$ at $\alpha = 28$ deg and $\Phi = 40$ deg, respectively, for thick wing.

round leading edges, if any, is not clear. Comparison of the velocity field with that of wings with sharp leading edge will be presented later on in the paper.

B. Nonslender Wings

As the recent experiments for a nonslender wing with sweep angle of $\Lambda = 50$ deg and sharp leading edges [12] showed roll oscillations, we investigated the roll response of various sharp-edged nonslender delta wings with different sweep angle. Figures 8a–8e show how the mean roll angle varied with angle of attack for nonslender wings with increasing sweep angle (from 40 up to 55 deg), with error bars showing the standard deviation of the roll angle time history. It is seen that, for low sweep angles, the mean roll angle is nonzero until a certain angle of attack is reached. These nonzero roll angles are consistent with the findings of previous work for sweep angles of 45 [9] and 50 deg [12]. In fact, the trim angle for the 45 deg wing at $\alpha = 20$ deg is at $\Phi_{\text{mean}} = 38$ deg, which correlates well with the data for a sharp leading-edged 45 deg delta wing in [9] in which a trim angle of $\Phi_{\text{mean}} = 40$ deg was obtained, albeit at a slightly lower Reynolds number of 2.2×10^5 in comparison to the 3.45×10^5 in our experiments (see Table 1). These nonzero roll angles are caused by the asymmetric reattachment of shear layers as shown by the tuft visualization pictures in [12]. It is seen in Fig. 8 that the mean roll angle drops to zero suddenly at a critical angle. For larger angles of attack, the roll angle remains as zero with virtually no fluctuations in the roll angle. The tuft visualization pictures [12] confirmed that there is no reattachment of the shear layers from either side. Hence, we called this behavior "stall of the free-to-roll wing." The stall angle increases with increasing sweep angle and is very sudden for nonslender wings. It is also interesting that the separated shear layers and vortex shedding do not cause any roll oscillations after the stall.

A second, more important point can be gleaned from the standard deviation values. It can be seen that as sweep angle increases a region of high standard deviation, corresponding to self-excited roll oscillations, develops just before stall. This is most noticeable in Figs. 8d and 8e, for sweep angles of 52.5 and 55-deg. If the angle of attack is increased beyond this region, the oscillations die out just before the wing stalls and the mean roll angle was seen to snap to zero. Examples of these oscillations for the cases of 52.5 and 55 deg sweep angles are shown in Figs. 9a and 9b. The self-excited roll oscillations in these cases exhibit some amplitude modulation, as previously seen for a wing with round leading edges [8–10,12,13] and of a constant frequency.

C. Slender Wings

Figures 10a–10d show how the mean roll angle varied with angle of attack for wings with sweep angles of 57.5, 60, 65, and 70 deg, again with error bars showing the standard deviation of the roll time history. As can be seen, the mean roll angle reduced to zero much more gradually with increasing angle of attack compared with the nonslender wings. In other words, the stall of the free-to-roll wing

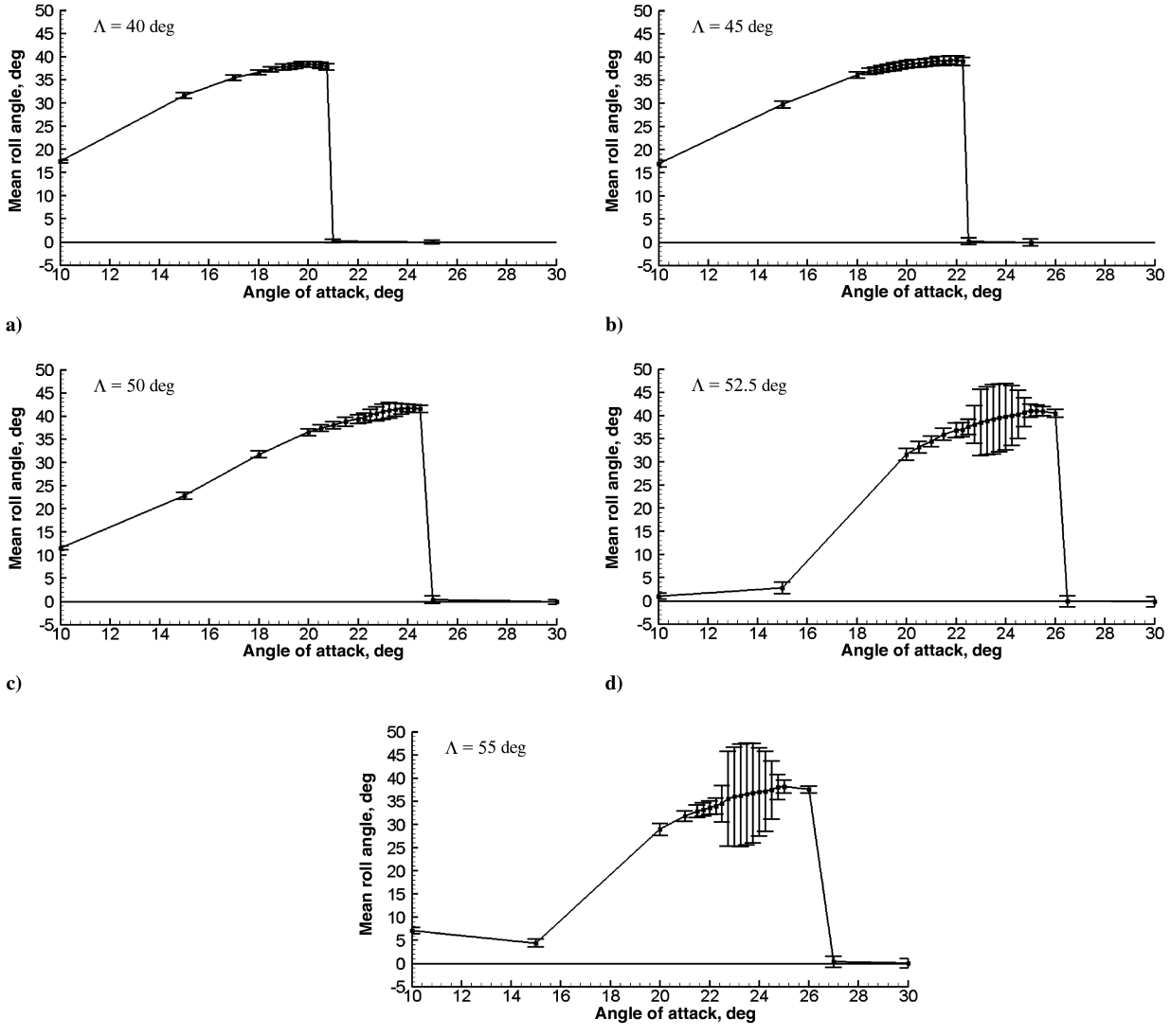

Fig. 8 Variation of mean roll angle as a function of angle of attack, with standard deviation as error bars, for thin wings with sharp leading edges.

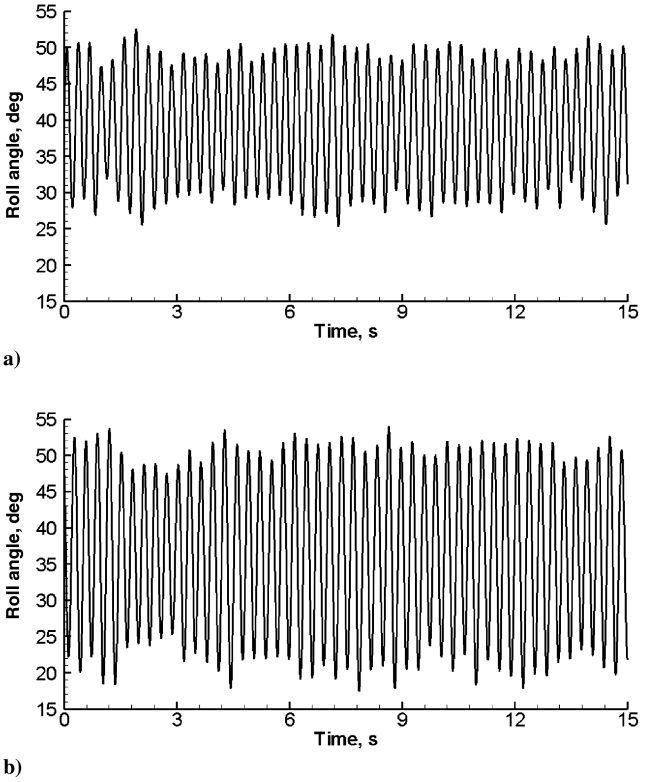

Fig. 9 Time history of roll angle corresponding to maximum standard deviation (at $\alpha = 23.5$ and 23.25 deg, respectively) for thin wings with a) $\Lambda = 52.5$ deg, and b) $\Lambda = 55$ deg.

becomes more gradual with increasing sweep angle. The magnitude of the nonzero mean roll angle decreases with increasing sweep angle, and becomes nearly zero for the most slender wing with $\Lambda = 70$ deg. This is attributed to the inability of the flow to reattach on slender wings [14]. The mean roll angles of the 60 and 65 deg wings at $\alpha = 30$ deg were both 18 deg, whereas Jenkins et al. [4] and Pamadi et al. [15] found slightly larger trim angles at the same angle of attack, with $\Phi_{\text{mean}} = 21$ deg for both sweep angles. This may be due to different Reynolds numbers.

In Figs. 10a and 10b, corresponding to wings with $\Lambda = 57.5$ and 60 deg, respectively, a region with large, self-excited oscillations can again be seen just before the mean roll angle starts decreasing, suggesting they might be caused by the same phenomenon as in the nonslender case. These oscillations die away with increasing angle of attack, before an interesting second region of high standard deviation is seen, after which the wing becomes fully stalled. This second region will be discussed further later on. For the $\Lambda = 65$ and 70 deg wings, the roll oscillations are very small. Figures 11a–11d show the roll angle time histories corresponding to the highest standard deviations from Fig. 10. The characteristics of the oscillations for the 57.5 and 60 deg wings were similar to those of the 52.5 and 55 deg wings in nature, and the oscillations were seen to die away with increasing sweep angle. The 65 and 70 deg wings again show slight unsteadiness but no periodic oscillations.

Combining the above results, the variation of the mean roll angle at maximum standard deviation and the standard deviation of roll angle itself are plotted against sweep angles in Figs. 12a and 12b, respectively. From Fig. 12a it can be seen that a maximum mean roll angle was seen for a wing of 50 deg sweep, whereas Fig. 12b shows that a peak standard deviation was seen for a wing of 57.5 deg sweep. Figure 13 shows how the Strouhal number of the wings with large oscillations varied with angle of attack. Slight increases were seen with increasing angle of attack in a similar manner to the moderate increases in reduced frequency that were observed with angle of attack during slender wing rock [1]. The increase for the thick wing was less, and the frequency was lower than that of the thin wings with sharp leading edges.

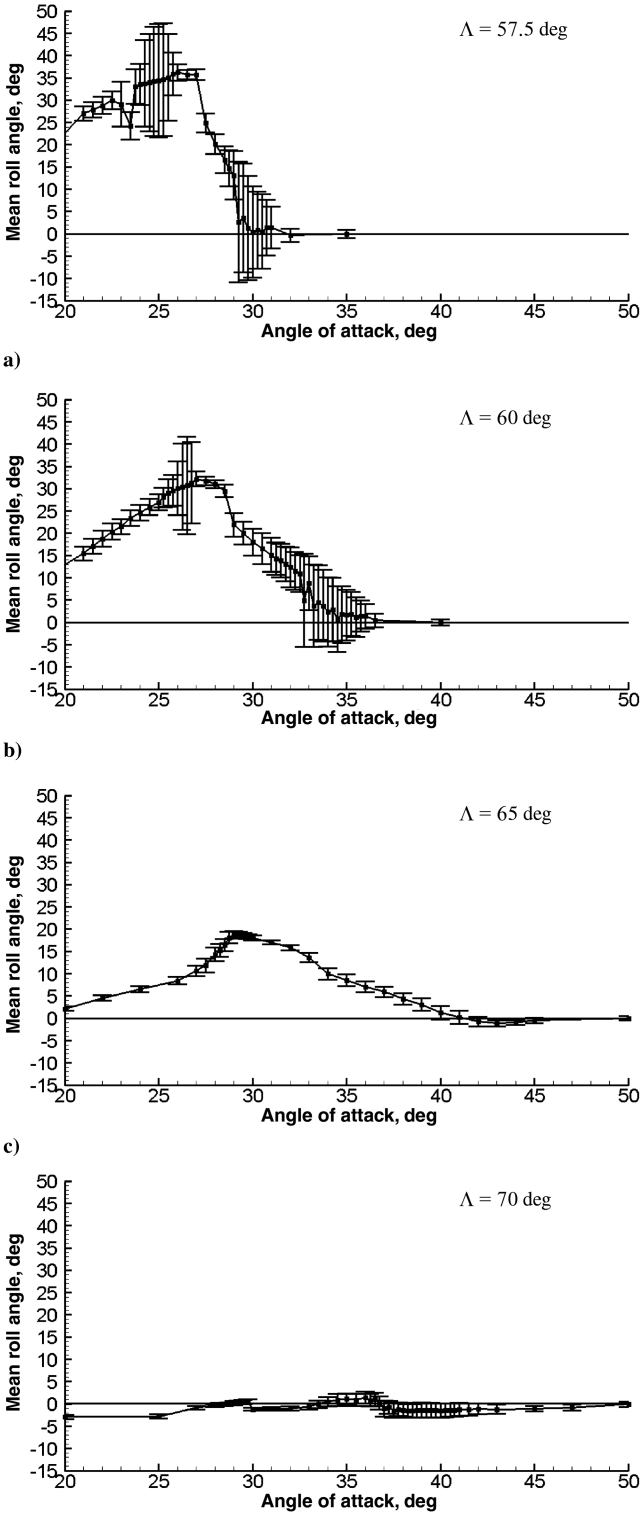

Fig. 10 Variation of mean roll angle as a function of angle of attack, with standard deviation as error bars, for thin wings with sharp leading edges.

D. Vortex Topology

Figure 14 shows how the velocity field changed in a crossflow plane as the angle of attack was increased for the 55 deg wing at $x/c = 0.25$, with the wing clamped at the mean roll angle obtained from the free-to-roll time histories. In part i, which is significantly before the self-excited oscillations, the reattachment points of either shear layer can be seen to be well separated. When α was increased to 22.25 deg in part ii, which is just before the self-excited roll

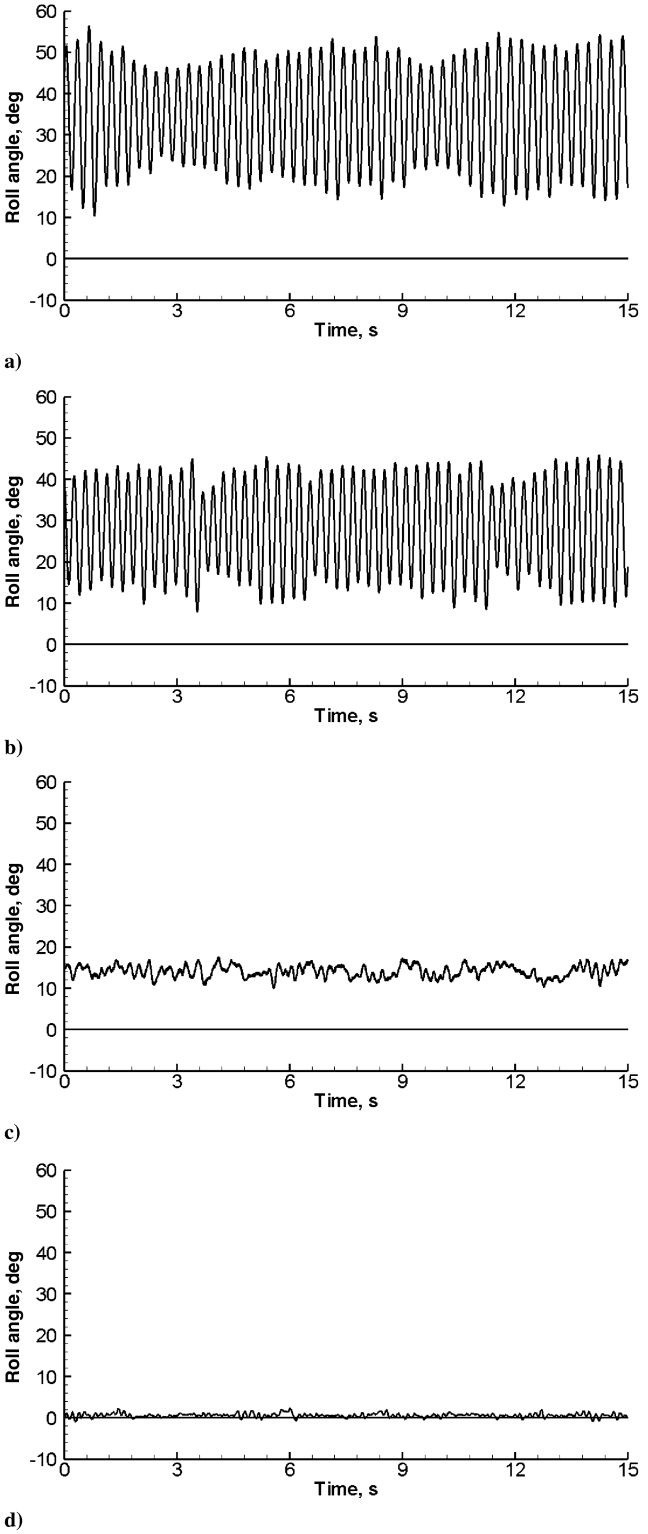

Fig. 11 Time history of roll angle corresponding to maximum standard deviation (at $\alpha = 25, 26.5, 28$ and 29.75 deg, respectively) for thin wings: a) $\Lambda = 57.5$ deg, b) $\Lambda = 60$ deg, c) $\Lambda = 65$ deg, and d) $\Lambda = 70$ deg.

oscillations begin, the right-hand side reattachment point was seen to move inboard. The increasing proximity of the shear layers may be what triggers these oscillations. In part iii, which would correspond to where large oscillations would be observed in the free-to-roll case, the reattachment points and thus shear layers can be seen to be very close together. For these three cases, the left-hand vortex appeared to be of a similar size. Finally, in part iv, which was just before the wing snapped to zero mean roll angle, the right-hand shear layer was seen to merge with the left-hand vortex and the two separate reattachment

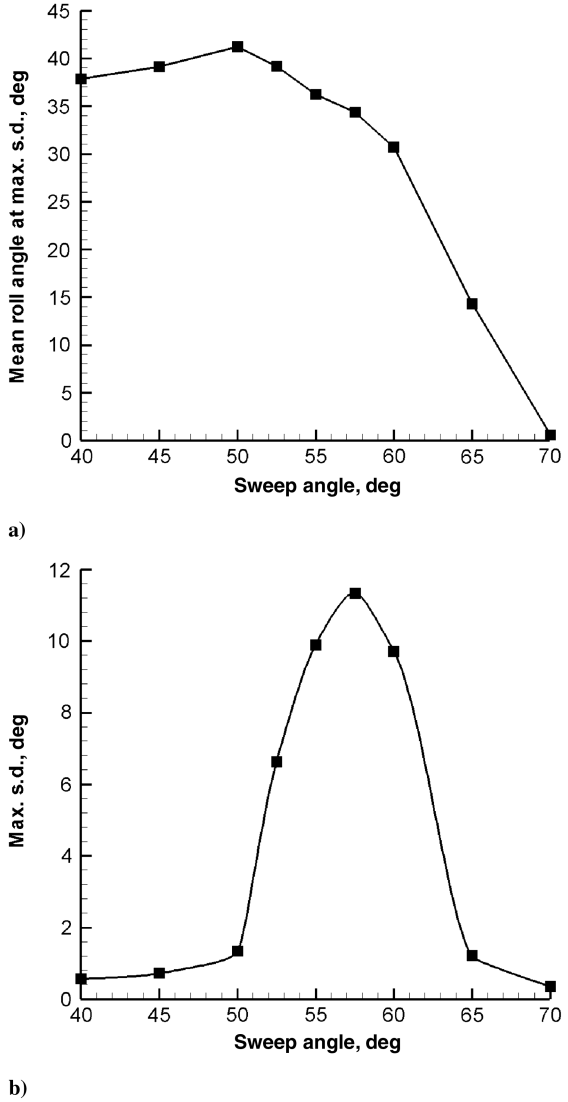

Fig. 12 Variation of a) mean roll angle at angle of attack with highest standard deviation and b) maximum standard deviation as a function of sweep angle for thin wings.

lines were replaced by one reattachment line. It is suspected that this increased separation region on the right-hand side with increasing angle of attack is a precursor of the sudden stall shown in the inset of Fig. 14.

In Fig. 15, dynamic PIV tests are presented at $\alpha = 23.75$ deg (corresponding to near maximum standard deviation in Fig. 8e) and $x/c = 0.5$ to gain an understanding of how the flow structure over the wing changes as the wing rolls. A timing diagram is included to clarify where the images were taken. Measurements near $\Phi_{\max}$ [(i)

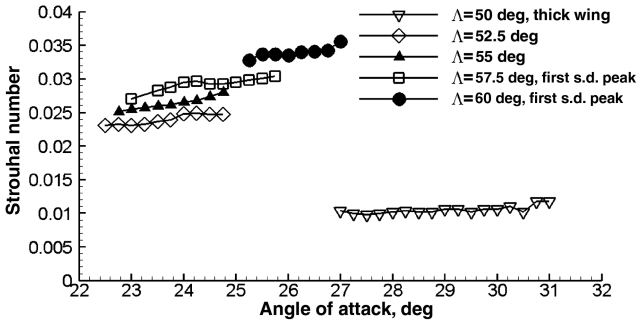

Fig. 13 Variation of Strouhal number with angle of attack for self-induced roll oscillations.

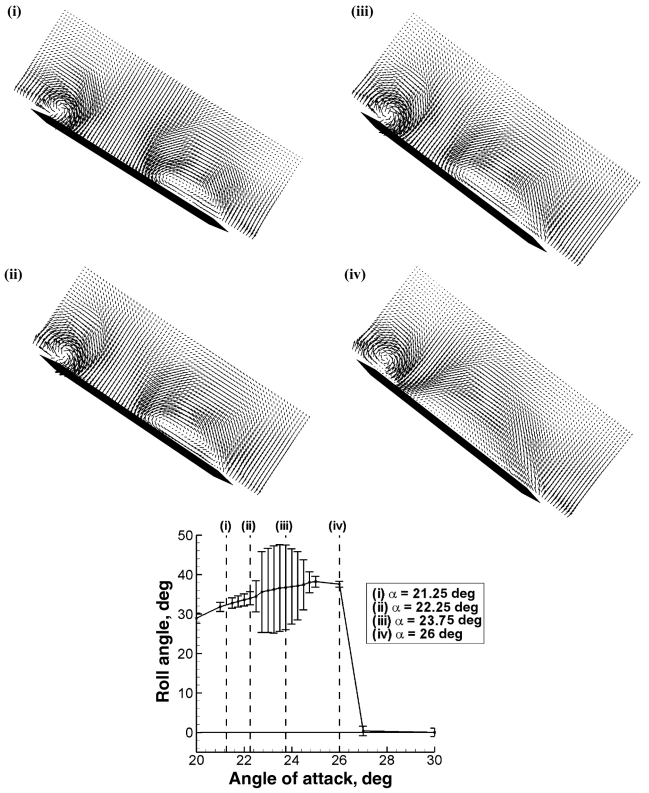

Fig. 14 Crossflow velocity field for stationary wing and graph of mean roll angle with standard deviation as error bars against angle of attack corresponding to images for thin wings with $\Lambda = 55$ deg at $x/c = 0.25$.

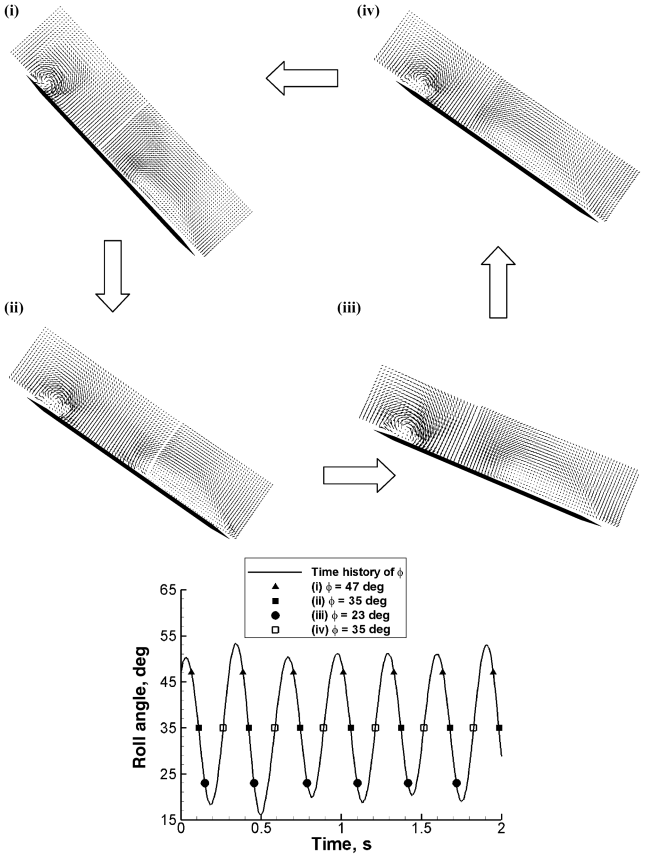

Fig. 15 Phase-averaged crossflow velocity fields and timing diagram corresponding to images for thin wings with $\Lambda = 55$ deg at $x/c = 0.5$ and $\alpha = 23.75$ deg.

$\Phi = 47$ deg] and near $\Phi_{\min}$ [(iii) $\Phi = 23$ deg] are shown, together with two more measurements at Φ_{mean}, one with roll angle decreasing and the other with roll angle increasing. At (i) a large reattached region exists. The left-hand vortex in this case appears to be compact and a right-hand vortical structure is close to the wing surface. As the roll angle decreased to (ii), the reattachment points were seen to move closer together and closer still in (iii) in which the wing was near the minimum roll angle. At this point the right-hand shear layer is further from the wing surface than it was at (i), which will reduce the lift generated from this wing half, and the left-hand vortex also appears to be much larger. Whether this is due to vortex breakdown, increased vortex strength because of increased effective angle of attack, or a combination of the two is not clear. The right-hand wing half is expected to have breakdown at the apex at all roll angles. As the roll angle again increases toward $\Phi_{\max}$, at (iv), the right-hand shear layer seems to be closer to the wing surface than at (iii) and it appears to reattach further inboard compared to (ii). Again, this shows the hysteresis effect. Overall, these features are similar to those for the thick wing discussed earlier.

In a similar manner to the 55 deg wing, Fig. 16 shows PIV measurements for the static wing taken at $x/c = 0.25$ and various angles of attack for the 60 deg sweep wing. The wing was clamped at the mean roll angle obtained from the free-to-roll time histories. At (i), which is before the oscillations commence, the reattachment points are seen to be separate. As the angle of attack was increased to 25.5 deg, point (ii), the reattachment points appeared to be very close. Finally, at (iii), which corresponds to the largest standard deviation, the right-hand shear layer now appears to be very close to the left-hand side vortex, and the flow on the right-hand side appears to be stalled. This is slightly different to what was observed with the 55 deg wing and can be attributed to the larger sweep angle, meaning the shear layers are closer to one another.

Figure 17 presents the phase-averaged measurements for the oscillating wing ($\Lambda = 60$ deg) at $x/c = 0.25$ and $\alpha = 26.5$ deg. At (i), near the maximum roll angle, the reattachment points are separated and it can be seen that the left-hand vortex is compact in

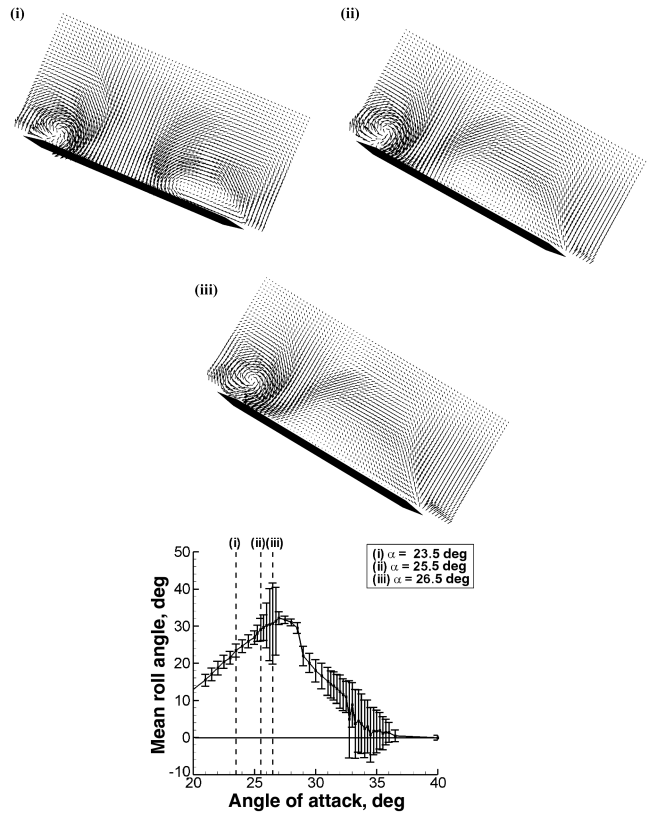

Fig. 16 Crossflow velocity field for stationary wing and graph of mean roll angle with standard deviation as error bars against angle of attack corresponding to images, for thin wings with $\Lambda = 60$ deg at $x/c = 0.25$.

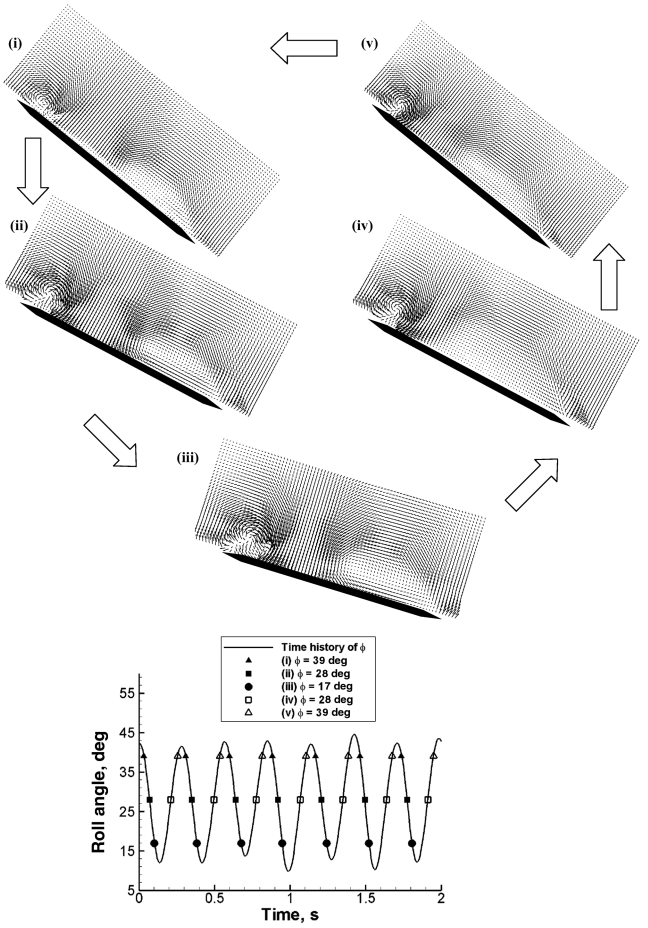

Fig. 17 Phase-averaged crossflow velocity and timing diagram corresponding to images for thin wings with $\Lambda = 60$ deg at $x/c = 0.25$ and $\alpha = 26.5$ deg.

this case. As the roll angle decreases to the mean value, at point (ii), the right-hand shear layer reattachment point is seen to move closer to the left-hand reattachment point, and closer still at (iii), which is near the minimum roll angle achieved during the motion. However, at the mean roll angle with roll angle increasing [point (iv)], the flow on the right-hand side stalls, which is interesting because it suggests a time lag exists between the minimum roll angle and wing stall. The wing recovers from this stall, and the right-hand shear layer reattaches before point (v) and again hysteresis is seen, as shown by a slightly different flow structure here compared with at point (i).

E. Different Modes of Oscillations

As discussed earlier, a second region of high standard deviation is seen to exist at high angles of attack for the 57.5 and 60 deg wings (see Fig. 10). Figure 18 shows roll angle time histories of the 60 deg wing through this region. Initially, at $\alpha = 33$ deg (Fig. 18a) self-excited oscillations develop again about a nonzero mean roll angle with a Strouhal number of $St = 0.031$. When the angle of attack is increased to 33.75 deg (Fig. 18b), the wing is seen to flip occasionally between the two mean roll angles. There is similarity to the earlier studies in which multiple trim positions are found [4,12]. This flipping between the two states is what causes the peak in the standard deviation in Fig. 10, though the oscillations alone at $\alpha = 33$ deg have a reasonably high standard deviation of around 4 deg, which is why PIV tests were performed at this angle of attack. The flipping increases in frequency as the angle of attack is increased further (Fig. 18c). With further increases in angle of attack, the mean roll angle becomes closer and closer to zero until the wing is fully stalled.

Figure 19 shows the velocity field near Φ_{max} [($\Phi = 12$ deg), left] and near Φ_{min} [($\Phi = 0$ deg), right] at $x/c = 0.25$ and $x/c = 0.5$ (in this figure every other velocity vector is omitted for clarity). It can

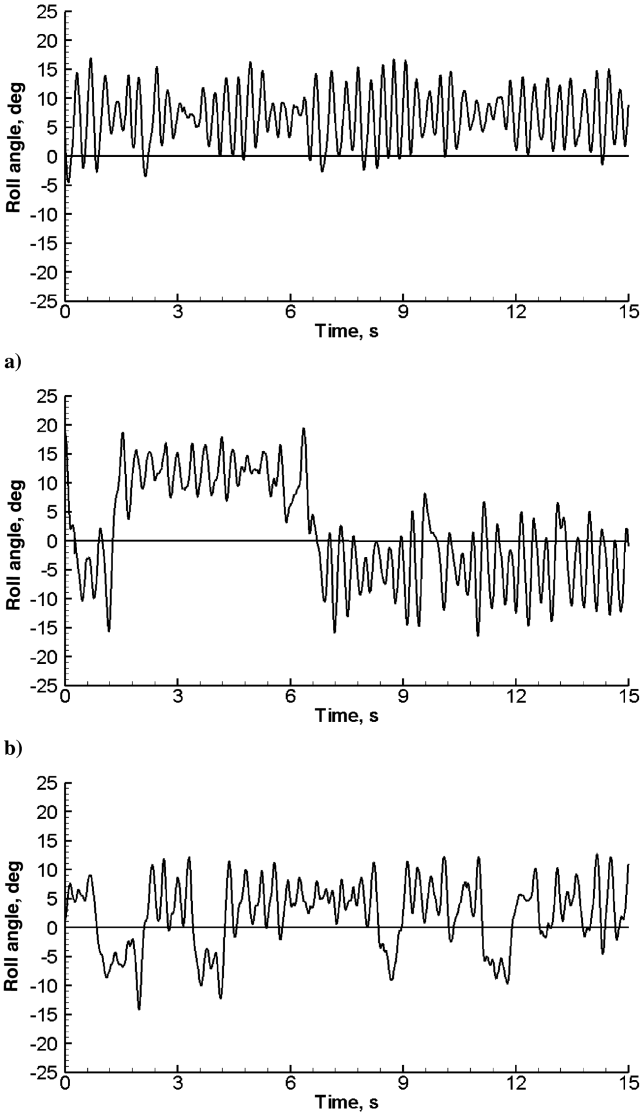

Fig. 18 Time history of roll angle at: a) $\alpha = 33$ deg, b) $\alpha = 33.75$ deg, and c) $\alpha = 35$ deg respectively, for wing with $\Lambda = 60$ deg.

clearly be seen at $x/c = 0.25$ that there is interaction between the shear layers near Φ_{max}, and this interaction can still be seen at $x/c = 0.5$. Near Φ_{min} a slightly asymmetric flow structure is present, demonstrating that a time lag exists as the flow structure at this roll angle of 0 deg is expected to be symmetrical for the static wing. It is worth noting that the distance between the reattachment locations (size of the reattached region) in this case seems to be out of phase with that of the first region of the oscillations. There appears to be minimum distance between the reattachment locations near the

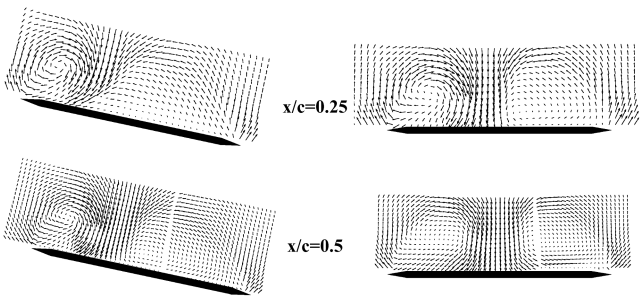

Fig. 19 Crossflow velocity fields near Φ_{max} (at $\Phi = 12$ deg left, and near Φ_{min} at $\Phi = 0$ deg right) for thin wing with $\Lambda = 60$ deg at $\alpha = 33$ deg.

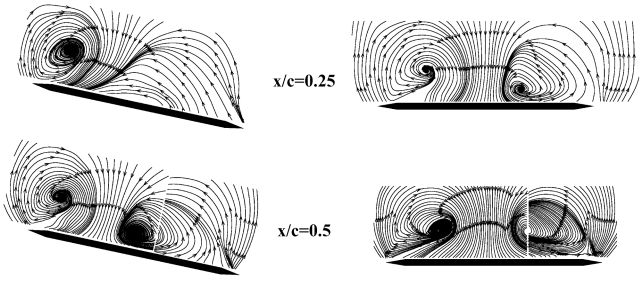

Fig. 20 Crossflow streamline patterns near Φ_{max} (at $\Phi = 12$ deg left, and near Φ_{min} at $\Phi = 0$ deg right) for thin wing with $\Lambda = 60$ deg at $\alpha = 33$ deg.

maximum roll angle, which is opposite to that of the oscillations in the first region. The right-hand shear layer reattaches further away nearer the maximum roll angle than the minimum roll angle, which is opposite to that in the first region.

The streamlines (Fig. 20) demonstrate the interaction between the shear layers near Φ_{max} and $x/c = 0.25$, and also the formation of a vortex on the right-hand wing half at $x/c = 0.5$. Near Φ_{min} the presence of vortical structures on both wing halves at both stations as well as the asymmetry in the flow at zero roll angle are confirmed. It can be seen that the right-hand vortical structure is further from the wing surface at $x/c = 0.5$ for Φ_{min} than at Φ_{max} and also slightly further inboard than the left-hand vortex. Figures 19 and 20 also indicate that the crossflow patterns are somewhat different in the two planes, suggesting that three-dimensional effects may exist. These effects may be important for the second mode of oscillations.

F. Possible Mechanisms of Oscillations

The mechanism for the roll oscillations of the thick wing with rounded leading edge and sweep angle of 50 deg, and the thin wings with sharp leading edges and sweep angles of 55 and 60 deg (first standard deviation peak) is thought to be the same. Before the roll oscillations are observed, nonzero roll trim angles are found. With increasing angle of attack, the reattachment lines move closer to each other similar to those on nonslender wings at zero roll angle [16], but at a much faster rate in the neighborhood of the onset of the oscillations. There appears to be an interaction between the left-hand and right-hand shear layers. The oscillations may be initiated by the increasing proximity of the shear layers as the angle of attack is increased. Self-excited roll oscillations can occur for fixed separation points. Reattachment is likely to be the main source, but separation on rounded leading edge also contributes.

Once the roll oscillations are developed, in all cases, a compact left-hand vortex is present near Φ_{max}. The presence of the right-hand vortex close to the wing surface generates more lift than the compact left-hand vortex and provides a restoring moment, which drives the wing in the other direction. As Φ decreases, the reattachment point of the right-hand shear layer moves closer to the left-hand shear layer reattachment point. At Φ_{min} the shear layer reattachment points are close to each other and the subsequent motion is driven by the stronger left-hand vortex generating more lift. As Φ increases, the left-hand vortex becomes more compact, the reattachment points of both shear layers move further apart, and the right-hand shear layer moves closer to the wing surface as the wing approaches Φ_{max} when the sequence starts again. Hysteresis effects are present and significant in all cases for these roll oscillations, even though the Strouhal number is very low.

For the case of the 60 deg wing around the second standard deviation peak, there are similarities but also differences compared with the first region. The variation of the size of the left-hand vortex with roll angle is similar, but the variation of the reattachment location of the right-hand shear layer with roll angle is the opposite. The data suggest that at Φ_{min} both left-hand and right-hand shear layers form large vortical structures. The asymmetry in the strength of the vortices due to a time lag appears to drive the rolling motion. Further experiments (force and pressure measurements), numerical simulations such as in [17], and reduced-order models such as in [18] could be useful for further understanding of the roll oscillations about a nonzero mean.

IV. Conclusions

Experiments were conducted on a series of free-to-roll delta wings with sharp leading edges and sweep angles in the range of 40–70 deg, as well as on a thick delta wing with round leading edges and a sweep angle of 50 deg. For low sweep angles, nonzero trim angles are typical until the wing stalls after which the trim angle becomes zero (when the flow reattachment is no longer possible). The stall angle increases with increasing sweep angle and is very sudden for nonslender wings. The stall of the free-to-roll wing becomes more gradual with increasing sweep angle. The magnitude of the roll trim angle decreases with increasing sweep angle and reaches zero at $\Lambda = 70$ deg. This can be attributed to the reattachment lines moving to the centerline with increasing sweep angle.

In a certain range of sweep angles (52.5–60 deg) and, just before the stall, large self-induced roll oscillations were seen for the wings with sharp leading edges. PIV measurements suggest that the oscillations are initiated by the increasing proximity of the shear layers as the angle of attack is increased. Self-exited roll oscillations occur for fixed separation point at the leading edge, but seem to be amplified when the separation is not fixed on rounded leading edges. The maximum standard deviation of the roll oscillations was found for a 57.5 deg sweep wing. There are two different regions of angles of attack for which the wing oscillated for $\Lambda = 57.5$ and 60 deg.

Phase-averaged PIV measurements showed that the mechanism for the roll oscillations of the thick wing with rounded leading edge and sweep angle of 50 deg, and the thin wings with sharp leading edges and sweep angles of 55 and 60 deg (first standard deviation peak) is the same. A strong vortex on the left-hand wing half drives the motion near the minimum roll angle Φ_{min}, whereas at Φ_{max} the restoring moment is created by the earlier reattachment of the right-hand shear layer (which becomes much closer to the wing surface), combined with a much smaller left-hand vortex. Hysteresis effects are significant even though typical Strouhal numbers are very low. A slightly different mechanism was revealed by the PIV measurements for the 60 deg wing in the second region of angle of attack in which the wing oscillated. These oscillations showed a different behavior of the right-hand shear layer, although the growth and decay cycle of the left-hand vortex during the roll oscillations is similar. In this case, it is suggested that asymmetry in vortex strength caused by a time lag provides the driving motion for the roll oscillations.

Acknowledgments

This work is sponsored by the U.S. Air Force Office of Scientific Research, Air Force Materiel Command, U.S. Air Force, under grant number FA8655-06-1-3058, and also by the Research Councils United Kingdom Academic Fellowship in Unmanned Air Vehicles.

References

[1] Levin, D., and Katz, J., "Dynamic Load Measurements with Delta Wings Undergoing Self-Induced Roll Oscillations," *Journal of Aircraft*, Vol. 21, No. 1, 1984, pp. 30–36. doi:10.2514/3.48218

[2] Arena, A. S., and Nelson, R. C., "Experimental Investigations on Limit Cycle Wing Rock of Slender Wings," *Journal of Aircraft*, Vol. 31, No. 5, 1994, pp. 1148–1155. doi:10.2514/3.46625

[3] Katz, J., "Wing/Vortex Interactions and Wing Rock," *Progress in Aerospace Sciences*, Vol. 35, No. 7, 1999, pp. 727–750. doi:10.1016/S0376-0421(99)00004-4

[4] Jenkins, J. E., Myatt, J. H., and Hanff, E. S., "Body-Axis Rolling Motion Critical States of a 65 Degree Delta Wing," *Journal of Aircraft*, Vol. 33, No. 2, 1996, pp. 268–278. doi:10.2514/3.46933

[5] Hanff, E. S., and Huang, X. Z., "Roll-Induced Cross-Loads on a Delta Wing at High Incidence," AIAA Paper 1991-3223, Sept. 1991.

[6] Huang, X. Z., and Hanff, E. S., "Prediction of Normal Force on a Delta Wing Rolling at High Incidence," AIAA Paper 93-3686, Aug. 1993.

[7] Gordnier, R. E., and Visbal, M. R., "Numerical Simulation of Delta-

Wing Roll," *Aerospace Science and Technology*, Vol. 2, No. 6, Sept. 1998, pp. 347–357.
doi:10.1016/S1270-9638(99)80023-6

[8] Ueno, M., Matsuno, T., and Nakamura, Y., "Unsteady Aerodynamics of Rolling Thick Delta Wing with High Aspect Ratio,"AIAA Paper 98-2520, June 1998.

[9] Matsuno, T., and Nakamura, Y., "Self-Induced Roll Oscillation of 45 Degree Delta Wings," AIAA Paper 2000-0655, Jan. 2000.

[10] Matsuno, T., Yokouchi, S., and Nakamura, Y., "The Effect of Leading-Edges Profile on Self-Induced Oscillations of 45 Degree Delta Wings," AIAA Paper 2000-4004, Aug. 2000.

[11] Ericsson, L. E., "Wing Rock of Non-Slender Delta Wings," *Journal of Aircraft*, Vol. 38, No. 1, 2001, pp. 36–41.
doi:10.2514/2.2731

[12] McClain, A., Wang, Z.-J., Vardaki, E., and Gursul, I., "Unsteady Aerodynamics of Free-to-Roll Non-Slender Delta Wings," AIAA Paper 2007-1074, Jan. 2007.

[13] Gursul, I. A., Gordnier, R., and Visbal, M., "Unsteady Aerodynamics of Non-Slender Delta Wings," *Progress in Aerospace Sciences*, Vol. 41, No. 7, 2005, pp. 515–557.
doi:10.1016/j.paerosci.2005.09.002

[14] Gursul, I., Wang, Z., and Vardaki, E., "Review of Flow Control Mechanisms of Leading-Edge Vortices," *Progress in Aerospace Sciences*, Vol. 43, No. 7–8, 2007, pp. 246–270.
doi:10.1016/j.paerosci.2007.08.001

[15] Pamadi, B. N., Rao, D. M., and Niranjana, T., "Wing Rock and Roll Attractor of Delta Wings at High Angles of Attack," AIAA, Paper 94-0807, Jan. 1994.

[16] Taylor, G., and Gursul, I., "Buffeting Flows over a Low Sweep Delta Wing," *AIAA Journal*, Vol. 42, No. 9, Sept 2004, pp. 1737–1745.
doi:10.2514/1.5391

[17] Arthur, M. T., Allan, M. R., Ceresola, N., Kompenhans, J., Fritz, W., Boelens, O. J., and Pranata, B. B., "Exploration of the Free Rolling Motion of a Delta Wing Configuration in a Vortical Flow," *RTO-MP-AVT-123, Flow Induced Unsteady Loads and the Impact on Military Application*,NATO, Rept. RTP-MP-AVT-123, Budapest, Hungary, April 2005.

[18] Badcock, K. J., Woodgate, M. A., Allan, M. R., and Beran, P. S., "Wing-Rock Limit Cycle Oscillation Prediction Based on Computational Fluid Dynamics," *Journal of Aircraft*, Vol. 45, No. 3, May–June 2008, pp. 954–961.
doi:10.2514/1.32812